Modelling the Effect of Intracellular Calcium in the Rundown of L-Type Calcium Current

Aditi Agrawal[1], Michael Clerx[2], Ken Wang[3], Liudmila Polonchuk[3], David J. Gavaghan[1], Gary R. Mirams[2]

[1] University of Oxford, Oxford, United Kingdom
[2] University of Nottingham, Nottingham, United Kingdom
[3] F. Hoffmann-La Roche Ltd., Basel, Switzerland

Abstract

The L-type calcium current (I_{CaL}) is a key current of the heart playing an important role in the contraction of the cardiomyocyte. Patch-clamp recordings of ionic currents can be associated with a reduction of the current magnitude with time (termed 'rundown'), and this phenomenon is particularly pronounced for I_{CaL} recordings. Some part of rundown can be attributed to the unique sensitivity of L-type calcium channels (LCCs) to local $[Ca^{2+}]$. In this paper, we study the experimental conditions in which rundown due to calcium-dependent inactivation (CDI) is minimised. We use first principles to derive an analytical equation for the diffusion of a calcium-chelating buffer from a patch hole on the cell's surface to the entirety of the cell. This determines the concentration profile of the buffer with respect to time and space. We then use the equation to simulate the effects of incoming calcium via the LCCs and its chemical reaction with the buffer.

1. Introduction

Models of the L-type calcium current I_{CaL} [1] can be built by calibrating and validating them against current recorded from patch-clamp experiments. A difficulty in building I_{CaL} models using information-rich protocols such as those used previously for hERG [2, 3], lies in the interpretation of the recorded current which is attenuated with time (also called rundown). Rundown in I_{CaL} is attributed to several factors including inactivation of I_{CaL} channels (LCCs) by local $[Ca^{2+}]$ (calcium-dependent inactivation, CDI), loss of phosphorylating agents (e.g. ATP) which facilitate the up-regulation of I_{CaL}, and activation of $[Ca^{2+}]$-dependent enzymes that eventually can cause LCCs proteolytic degradation [4]. One way in which CDI-induced rundown is known to be reduced in patch-clamp experiments is by using $[Ca^{2+}]$-chelating buffers (e.g. BAPTA, EGTA) in the cell's internal solution. Nevertheless, some amount of rundown remains in such recordings.

In this study we model the experimental conditions at which CDI-induced rundown is minimised by accounting for the amount of calcium brought into the cell by I_{CaL}, diffusion of the $[Ca^{2+}]$-chelating buffer ($[B]$), and the chemical reaction of the $[Ca^{2+}]$ and $[B]$ in a whole-cell patch-clamp voltage-clamp experiment.

2. Methods and results

In this section we set up the geometrical problem of the buffer and its entry into the cell; and subsequently use it to derive an analytical solution of the diffusion of buffer from the a punctured hole on the cell's surface to the entirety of the cell. Finally, we combine the effects of 1) entry of $[Ca^{2+}]$ via LCCs into the cell, 2) chemical reaction of $[Ca^{2+}]$ and $[B]$, and 3) diffusion of the three chemical species $[Ca^{2+}]$, $[B]$, and $[CaB]$ as per the concentration gradient reaction; in a numerical scheme according to the finite volume method to simulate I_{CaL} with time.

2.1. Shape and axis of symmetry of a suspended cell

We consider the Chinese hamster ovarian (CHO) cell utilised in an automated patch-clamp experimental system. CHO cells are placed on a well above a hole on a plate, suction applied at this hole ruptures the membrane and keeps the cell in place so that whole-cell patch clamp configuration is achieved. This results in the 'squashing' of the cell (Figure 1B) which is otherwise approximately spherical in shape (Figure 1A). Intracellular solution containing the buffer (shown in blue) enters the cell from this punctured patch hole.

This 'squashed' cell can be approximated as hemispherical in shape and it is easy to see that there are two axes of symmetry along which the buffer entering the cell diffuses, one along the radius (r), and the other along the

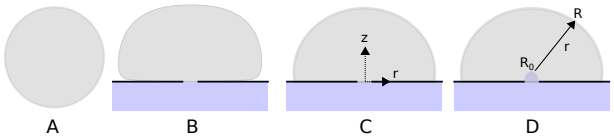

Figure 1. CHO cell A) Freely suspended, B) Ruptured and attached to the seal chip plate from which the intracellular solution enters the cell, C) hemi-spherical model of the patched cell and co-ordinate system, and D) hollow hemi-spherical model of the patched cell and co-ordinate system with the inner and outer radii.

axial direction (z) as shown in Figure 1C. The diffusion of the buffer in these cylindrical coordinates is given by the equations below:

$$\frac{\partial \mathrm{B}}{\partial t} = \frac{D_B}{r}\frac{\partial}{\partial r}\left(r\frac{\partial \mathrm{B}}{\partial r}\right) + D_B\frac{\partial \mathrm{B}}{\partial z}, \tag{1}$$

$$\begin{aligned}
&\mathrm{B}|_{z=0} = \mathrm{B}_{max} \qquad \text{if} \quad r \le R_0,\\
&\frac{\partial \mathrm{B}}{\partial z}|_{z=0} = 0 \qquad \text{if} \quad r > R_0,\\
&\frac{\partial \mathrm{B}}{\partial r}|_{r=0} = 0, \quad \text{and}\\
&\mathrm{B}|_{t=0} = \begin{cases} \mathrm{B}_{max} & r \le R_0 \quad \& \quad z = 0,\\ 0 & otherwise. \end{cases}
\end{aligned}$$

We check if, for the time duration of our experiment, these 2-D equations can be simplified to a 1-D spherical cell. We do this by discretising the equations using the finite volume method [5] on a 2-d mesh of 100 μm with 200 divisions in each direction.

Figure 2 shows the concentration gradient at 1 ms, 10 ms, and 100 ms from the start of the experiment. This figure shows that at longer times the diffusion becomes approximately radially symmetric. Therefore, we adopt a spherical axis of symmetry as shown in Figure 1D where we project the surface area of the planar hole in Figure 1C onto a hemi-spherical volume of equivalent curved surface area (radius = R_0).

Table 1. Constant values used for simulations in this paper.

Quantity	Variable	Value
Patch hole radius (μm)	R_0	$1/\sqrt{2}$
f_{Ca} half-concentration (μM)	K_{IC50}	3×10^{-4}
BAPTA concentration (mM)	$\mathrm{B}_{\mathrm{max}}$	10
BAPTA diffusion (cm^2/ms)	D_{B}	2×10^{-9} [6]
Backward BAPTA rate (1/ms)	k_{off}	0.298 [7]
Forward BAPTA rate (1/mM/ms)	k_{on}	1700 [7]

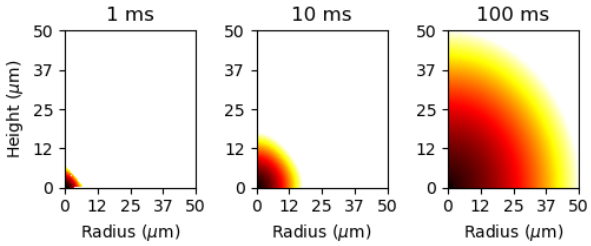

Figure 2. Contour map showing the diffusion of the buffer from the patch hole to the whole spherical cell. The maximum concentration of 10 mM is shown in black while concentration of 0 mM is shown in white. D_B and R_0 are given in Table 1.

2.2. Diffusion of buffer into the cell

We first consider the buffer concentration profile before the voltage-clamp is applied to the cell. Using the spherical shape and symmetry approximation as defined in the previous section, the diffusion of the free buffer (B) in spherical polar coordinates is given by:

$$\begin{aligned}
&\frac{\partial \mathrm{B}}{\partial t} = \frac{D_B}{r^2}\frac{\partial}{\partial r}\left(r^2\frac{\partial \mathrm{B}}{\partial r}\right),\\
&\mathrm{B}|_{r=R_o} = \mathrm{B}_{max},\\
&\frac{\partial \mathrm{B}}{\partial r}|_{r=R} = 0, \quad \text{and}\\
&B|_{t=0} = 0.
\end{aligned} \tag{2}$$

Next, we non-dimensionalise this partial differential equation (PDE) using $x = \frac{r-R}{R_o-R}$, $\tau = \frac{D_B t}{(R-R_o)^2}$, and $u(x,\tau) = \frac{\mathrm{B}r}{B_{max}R_o}$. These non-dimensionalised entities are now substituted into the PDE and the boundary equations to obtain:

$$\begin{aligned}
&\frac{\partial u}{\partial \tau} = \frac{\partial^2 u}{\partial x^2},\\
&u|_{x=1} = 1,\\
&\left[\frac{\partial u}{\partial x} - \frac{hu}{hx-1}\right]_{x=0} = 0, \quad \text{and}\\
&u|_{\tau=0} = 0;
\end{aligned} \tag{3}$$

where $h = 1 - \frac{R_o}{R}$. The general solution of Equation (3) is given by the trignometrical series [8]:

$$u(x,\tau) = f(x) + \sum_{n=1}^{\infty}[A_n \sin\lambda_n x + B_n \cos\lambda_n x]e^{-\lambda_n^2\tau}, \tag{4}$$

where $f(x)$ is a linear function determined by the diffusion profile at infinite time. Assuming that the buffer

will fully equilibrate to the entire cell in infinite time; $u(0,\infty) = \frac{1}{1-h}$, and $u(1,\infty) = 1$. Therefore, $f(x) = \frac{xh-1}{h-1}$. The variables A_n, B_n, and the eigenvalues λ_n can be determined using the boundary and initial conditions of Equation (3).

First applying the boundary condition at $x = 0$ to Equation (4), we get,

$$\sum_{n=1}^{\infty}(\lambda_n A_n + hB_n)e^{-\lambda_n^2\tau} = 0, \tag{5}$$

which is only possible if

$$\lambda_n A_n + hB_n = 0 \quad \text{and} \tag{6}$$

$$B_n = -\frac{\lambda_n A_n}{h}. \tag{7}$$

Next, applying the boundary condition at $x = 1$ to Equation (4), we get

$$\sum_{n=1}^{\infty}(A_n \sin\lambda_n + B_n \cos\lambda_n) = 0, \tag{8}$$

which is only possible if

$$A_n \sin\lambda_n + B_n \cos\lambda_n = 0. \tag{9}$$

Substituting equation (7) into this we obtain

$$\tan\lambda_n = \frac{\lambda_n}{h}, \tag{10}$$

which gives the solution to the eigenvalues of equation (4). Equation (10) does not have any analytical solution but has infinite numerical solutions and we consider positive roots of this equation to be the particular solutions of the PDE. Finally, applying the initial condition $u(x,0) = 0$ to Equation (4), we get:

$$-f(x) = \sum_{n=1}^{\infty} A_n F_n(x), \tag{11}$$

where $F_n(x) = \sin\lambda_n x - \frac{\lambda_n}{h}\cos\lambda_n x$. We then adopt the orthogonality condition derived by Lü & Bülow [8] using *Sturm-Liouville* theory [9] to determine the relationship:

$$\begin{aligned}
A_n &= -\frac{\alpha_n}{\beta_n}, \\
\alpha_n &= \frac{1}{h-1}\left[\left(\frac{1}{h} + \frac{h}{\lambda_n^2} - 1\right)\sin\lambda_n - \frac{h}{\lambda_n}\cos\lambda_n\right], \\
\beta_n &= \frac{1}{2h^2}\left[\lambda_n^2 + h^2 + \frac{\lambda_n^2 - h^2}{2\lambda_n}\sin 2\lambda_n - 2h\sin^2\lambda_n\right].
\end{aligned} \tag{12}$$

B_n can now be determined using equation (7) and equation (12) as:

$$B_n = -\frac{\lambda_n \alpha_n}{h\beta_n}. \tag{13}$$

The resultant analytical solution of the diffusion of the buffer is plotted for different τ in Figure 3, left.

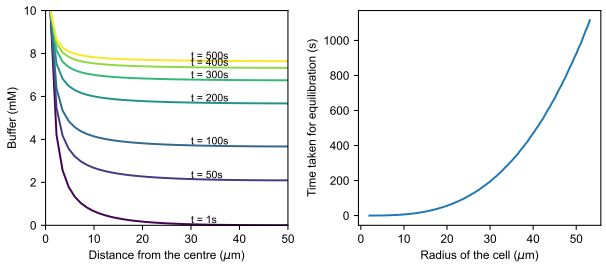

Figure 3. **Left**: Concentration profile of the buffer inside a cell with hemi-spherical geometry computed at different times ($R = 50\mu$m). **Right**: Time taken for near complete equilibration ($B \geqslant 0.99B_{max}$) at $r = R$ for cells of different sizes. Both the subplots have been generated using the analytical solution given by Equation (4) and the variable values in Table 1.

2.3. Chemical reaction & simulation of I_{CaL}

The analytical equation in the previous section is used to determine the concentration profile of the buffer before a voltage-clamp is applied. I_{CaL} channels on the surface of the CHO cell bring in $[Ca^{2+}]$ into the cell and it reacts with [B] to form the complex [CaB]. The net change in the species $[Ca^{2+}]$, [B], and [CaB] with time is given by the following ordinary differential equation (ODE) represented by the variable [X]:

$$\frac{\partial[\mathrm{X}]}{\partial t} = \overbrace{\frac{D_X}{r^2}\frac{\partial}{\partial r}\left(r^2\frac{\partial[\mathrm{X}]}{\partial r}\right)}^{\text{diffusion}} - \overbrace{(k_{\text{on}}\cdot[Ca^{2+}][\mathrm{B}] - k_{\text{off}}\cdot[\mathrm{CaB}])}^{\text{chemical reaction}}. \tag{14}$$

The diffusion term above was rewritten as a difference in flux followed by discretisation of the equations by adopting the finite volume method [5] and dividing the cell into N hemi-spherical shells of equal width. The $[Ca^{2+}]$ in the outermost shell affects the CDI of I_{CaL} [10], modelled by $f_{Ca} = 1/(1 + \frac{[Ca^{2+}]}{K_{IC50}})$.

These equations were then simulated using Myokit 1.33.0 [11] with CVODE 5.7.0 and the solver's relative and absolute tolerances were set to 10^{-7}. Figure 4 shows the simulated rundown using a voltage step protocol to 0 mV interspersed with a holding potential duration (t_{hold}) of 10 s

at -90 mV (inset). $[Ca^{2+}]$, f_{Ca}, and I_{CaL} recorded at each sweep are overlaid on top of each other showing the increase in $[Ca^{2+}]$-accumulation, causing decrease in amplitude of both f_{Ca} and I_{CaL} with time. Peak current at each sweep is plotted in the rightmost plot against the sweep number showing rundown.

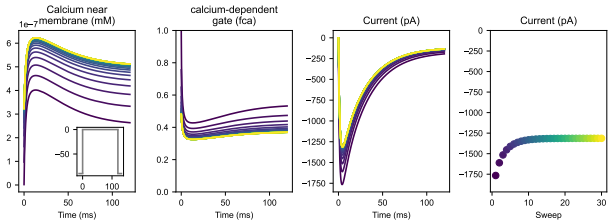

Figure 4. Simulated **A**: local $[Ca^{2+}]$ near the membrane with the step protocol inset, **B**: CDI gate (f_{Ca}), and **C**: I_{CaL} during the step up of V_m to 0 mV for successive sweeps with indigo and yellow corresponding to the first and last sweep respectively. **D**: peak-I_{CaL} at each sweep. Here $t_0 = 180$ s and $R = 30\mu$m.

3. Discussion and conclusion

In the previous section we picked arbitrary values of R, t_0, and t_{hold}. In real patch-clamp experiments R can vary from 2 to 43 μm and the corresponding t_{diff}'s range (Figure 3, left) is plotted on the number line in Figure 5. The conventional range for t_0 and t_{hold} in patch-clamp experiments is also shown in this figure.

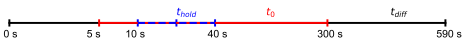

Figure 5. The range of possible values of t_{diff}, t_0, t_{hold}.

We repeated the simulations of I_{CaL} at various combinations of the three time time constants. Two types of rundown trends are predicted by the model—one in which a typical saturating rundown occurs due to CDI like that observed in Figure 4, the other is an 'inverse' rundown where the magnitude of I_{CaL} increases per sweep before saturating. We find that when the dimensionless quantity $\zeta = t_0^2/(t_{diff}t_{hold})$ is greater than 2, the rundown is of the first type, otherwise it is of the second type. Further, we find that when t_{diff} is the smallest time—there is almost no rundown, when t_0 is the smallest—the rundown is always inverse, and when t_{hold} is the smallest then rundown trend can be predicted using ζ. This indicates that CDI-induced rundown is directly affected by the amount of buffer available near the LCCs and how the depleted $[B]$ is being replenished. Repeated draws of the three time constants from the number line indicate that the probability of no-rundown conditions is less than 5%.

This work suggests that CDI-induced rundown can be avoided by using current recordings from small cells, or alternatively by increasing the inter-pulse duration and the initial time the buffer has to diffuse into the cell.

References

[1] Agrawal A, Wang K, Polonchuk L, Cooper J, Hendrix M, Gavaghan DJ, Mirams GR, Clerx M. Models of the cardiac l-type calcium current: a quantitative review. WIREs Mechanisms of Disease 2022;.

[2] Beattie KA, Hill AP, Bardenet R, Cui Y, Vandenberg JI, Gavaghan DJ, de Boer TP, Mirams GR. Sinusoidal voltage protocols for rapid characterisation of ion channel kinetics. The Journal of Physiology 2018;596(10):1813–1828.

[3] Lei CL, Clerx M, Gavaghan DJ, Polonchuk L, Mirams GR, Wang K. Rapid characterization of hERG channel kinetics I: using an automated high-throughput system. Biophysical Journal 2019;117(12):2438–2454.

[4] Belles B, Malecot CO, Hescheler J, Trautwein W. "rundown" of the Ca current during long whole-cell recordings in guinea pig heart cells: role of phosphorylation and intracellular calcium. Pflugers Archiv 1988;411(4):353–360.

[5] Fallah NA, Bailey C, Cross M, Taylor GA. Comparison of finite element and finite volume methods application in geometrically nonlinear stress analysis. Applied Mathematical Modelling 2000;24(7):439–455.

[6] Nowycky MC, Pinter MJ. Time courses of calcium and calcium-bound buffers following calcium influx in a model cell. Biophysical Journal 1993;64(1):77–91.

[7] Lattanzio Jr FA, Bartschat D. The effect of pH on rate constants, ion selectivity and thermodynamic properties of fluorescent calcium and magnesium indicators. Biochemical and Biophysical Research Communications 1991; 177(1):184–191.

[8] Lü Y, Bülow M. Analysis of diffusion in hollow geometries. Adsorption 2000;6(2):125–136.

[9] Kreyszig E, Stroud K, Stephenson G. Advanced engineering mathematics. Integration 2008;9:4.

[10] Zeng J, Laurita KR, Rosenbaum DS, Rudy Y. Two components of the delayed rectifier K^+ current in ventricular myocytes of the guinea pig type: Theoretical formulation and their role in repolarization. Circulation Research 1995; 77(1):140–152.

[11] Clerx M, Collins P, Lange Ed, Volders PG. Myokit: a simple interface to cardiac cellular electrophysiology. Progress in Biophysics and Molecular Biology 2016;120(1-3):100–114.

Address for correspondence:

Aditi Agrawal

Department of computer science, 7 Parks Road, Oxford OX1 3QG, United Kingdom

aditi.agrawal@cs.ox.ac.uk